Supplemental Information

The Influence of Peripheral Substituent Modification on P^V, Mn^{III}, and $Mn^V(O)$ Corrolazines: X-ray Crystallography, Electrochemical and Spectroscopic Properties, and HAT and OAT Relativities

*Evan E. Joslin, Jan Paulo T. Zaragoza, Regina A. Baglia, Maxime A. Siegler, and David P. Goldberg**

Department of Chemistry, The Johns Hopkins University, 3400 N. Charles Street, Baltimore, MD 21218, USA

*Email: dgp@jhu.edu

General Procedures. All reactions were preformed using dry solvents and standard Schlenk techniques unless otherwise noted. Methylene chloride-d_2 was obtained from Cambridge Isotopes, Inc. PPh_3 and $Bu_4N^+F^-$ (tetrabutylammonium fluoride) were purchased from commercial sources and used without further purification. **Instrumentation.** $^{31}P\{^1H\}$ NMR spectra were obtained on a Bruker 400 MHz (operating frequency 161.9 MHz) spectrometer and referenced against an external standard of H_3PO_4 ($\delta = 0$).

OAT Product Analysis. PPh_3 (10 equiv) was added by syringe to a CH_2Cl_2 solution of $Mn^V(O)(MeOP_8Cz)$ (1.13 mM). The solution went immediately from a deep green to a dark brown, indicating conversion to $Mn^{III}(MeOP_8Cz)(OPPh_3)$. The reaction was monitored by UV-Vis spectroscopy, which showed conversion to $Mn^{III}(MeOP_8Cz)$. An amount of $Bu_4N^+F^-$ (30 equiv) was then added to release the $OPPh_3$. The solution was then concentrated to dryness, reconstituted in CD_2Cl_2 (450 μL) and immediately analyzed by $^{31}P\{^1H\}$ NMR spectroscopy. The delay time (D1) was set to 150 s to allow for complete relaxation of the ^{31}P nucleus. Comparison of the integration for the peaks PPh_3 (δ = -5.5 ppm) and $OPPh_3$ (δ = 27.3 ppm) gave a yield of 77% for $OPPh_3$ (Figure S16).

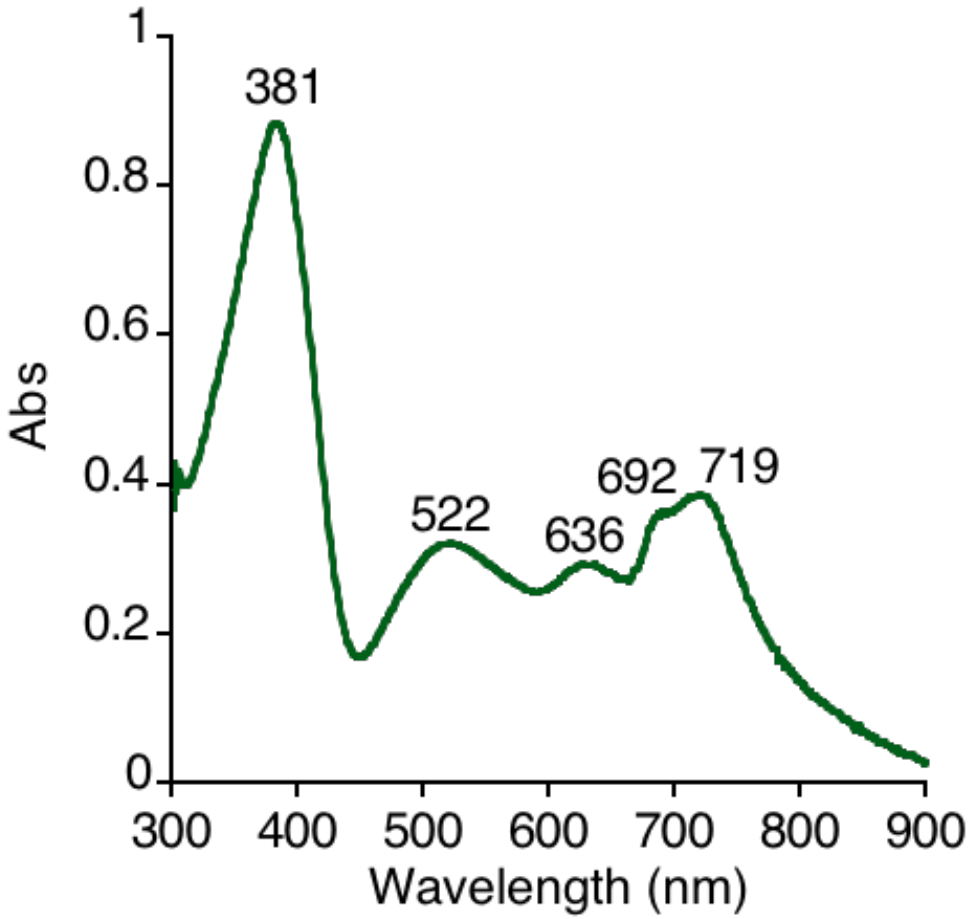

Figure S1. UV-vis spectrum of $MeOP_8PzH_2$ in pyridine.

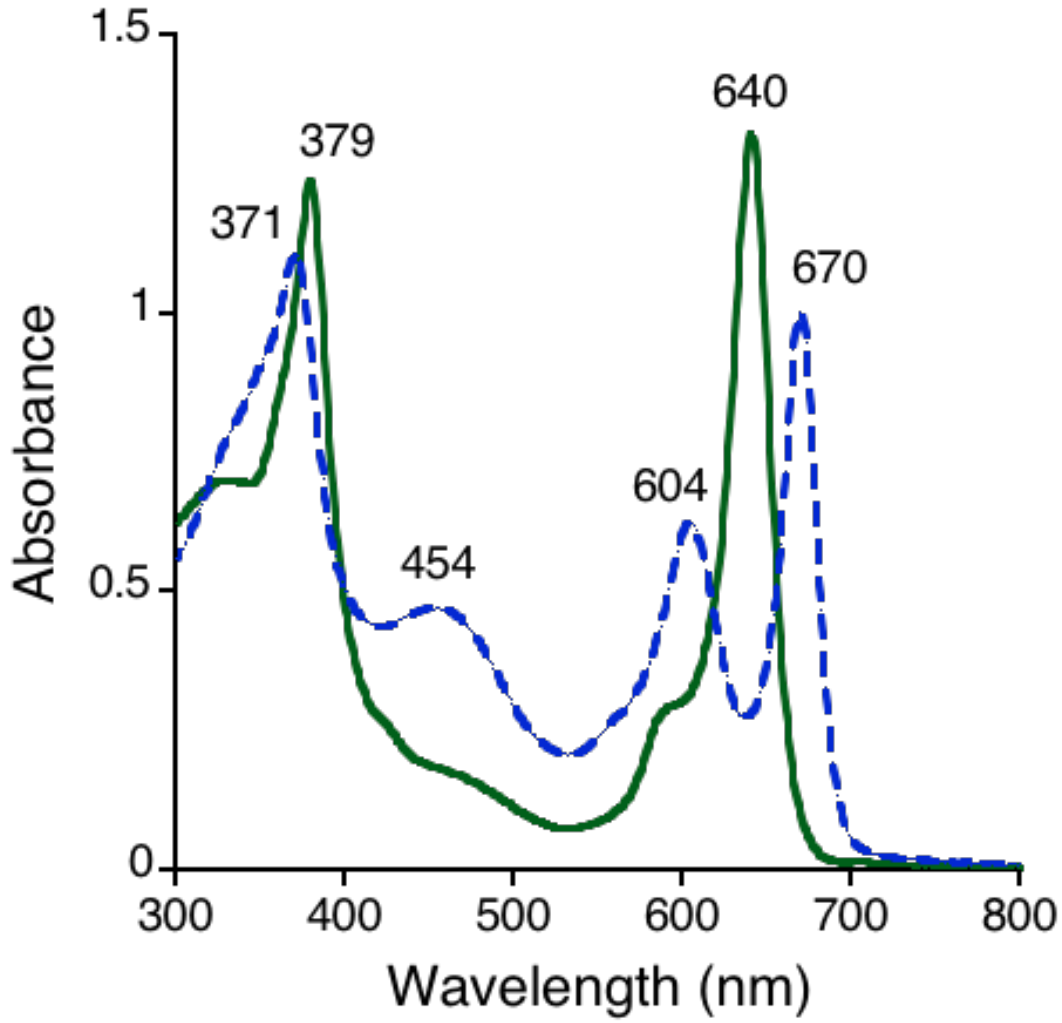

Figure S2. UV-vis spectrum of Mg(iPrP$_8$Pz) (solid green line) and iPr$_8$PzH$_2$ (dashed blue line) in CH_2Cl_2.

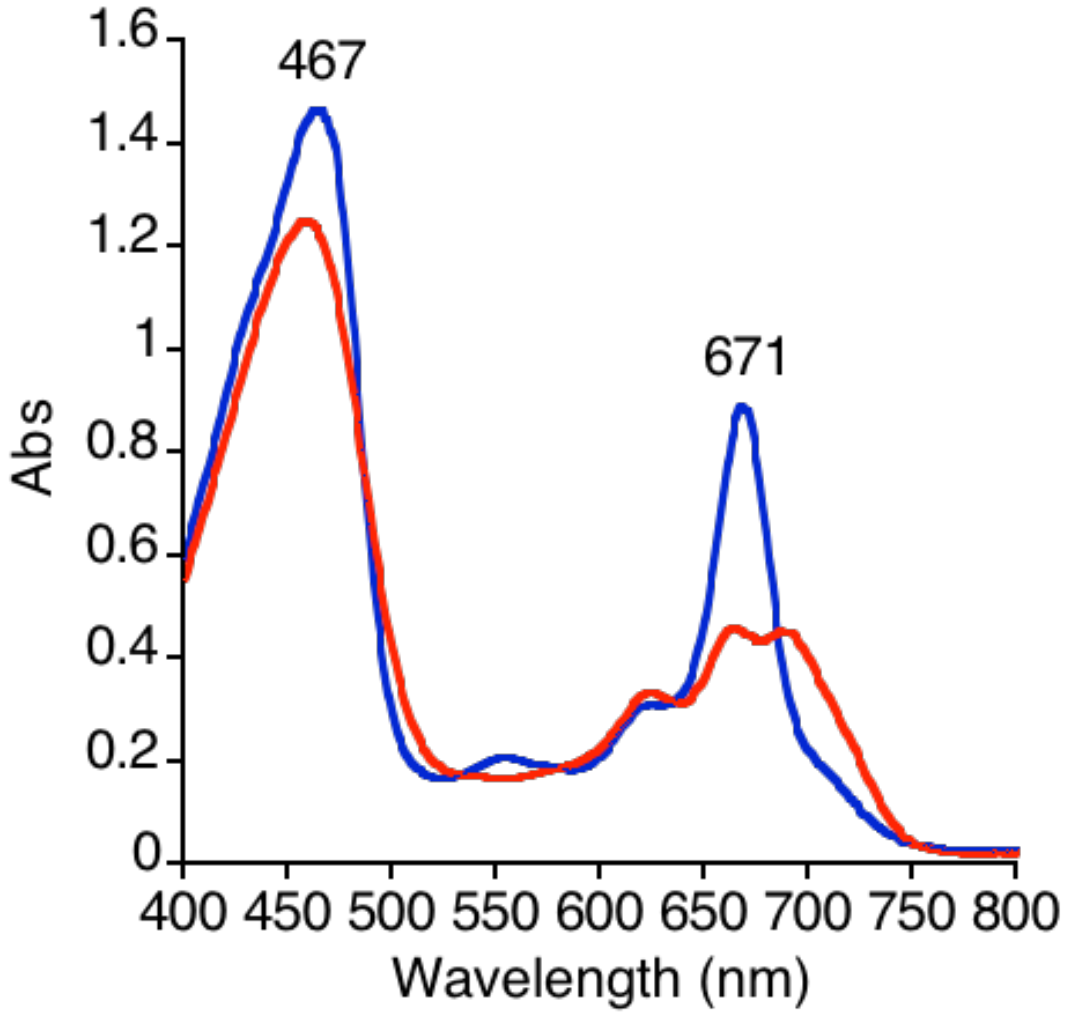

Figure S3. UV-vis spectrum of $MeOP_8CzH_3$ in pyridine (blue) and CH_2Cl_2 (red).

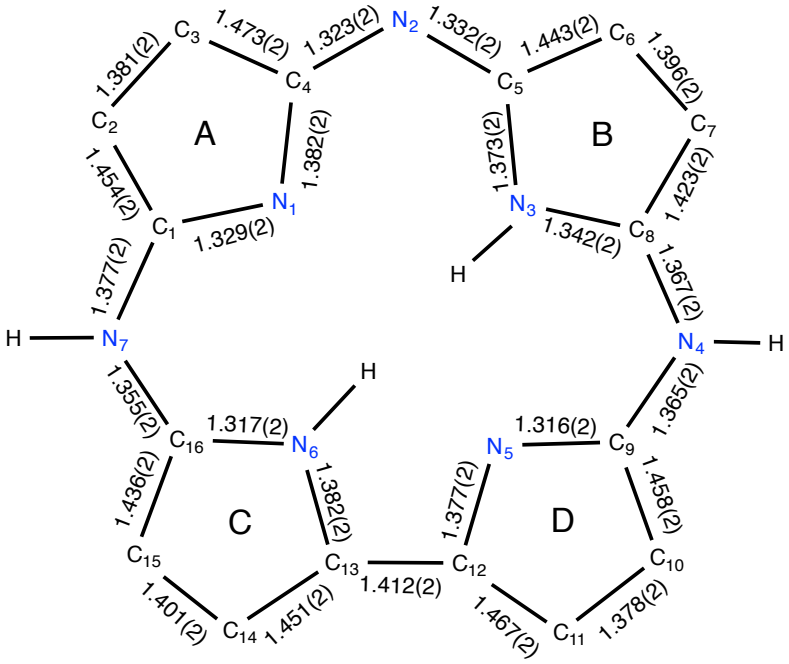

Figure S4. Bond lengths for the macrocyclic core of $[TBP_8CzH_4]^+$ cation determined by single crystal X-ray crystallography.

Table S1. Selected Bond Lengths (Å) for *t*-Bu corrolazine complexes.

	TBP_8CzMn^{III}	**$[TBP_8CzMn^{III}H][BArF]$**	**$[TBP_8CzMn^{III}H_2][BArF]_2$**	**$[TBP_8CzH][BArF]$**
C_β-C_β (av)	1.393(5)	1.385(7)	1.391(3)	1.389(2)
C_α-C_β (av)	1.447(5)	1.445(6)	1.442(3)	1.451(2)
C_α-C_α (C12-C13)	1.442(6)	1.454(6)	1.409(3)	1.412(2)
C_α-$N_{pyrrole}$ (av)	1.378(6)	1.370(6)	1.366(3)	1.352(2)
C_α-N_{meso} (av)	1.344(5)	1.348(7)	1.355(3)	1.353(2)

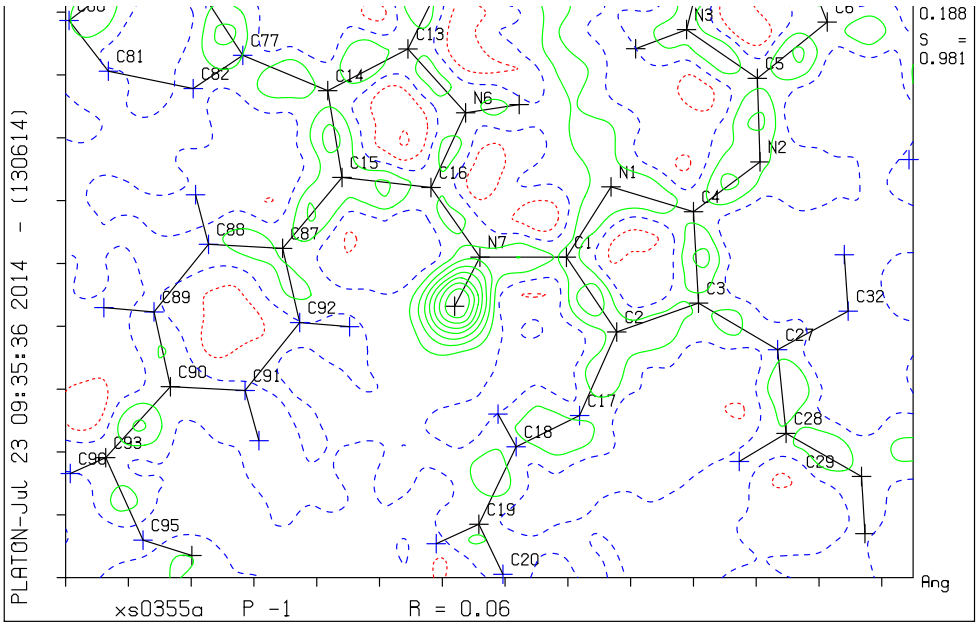

Figure S5. Electron density difference Fourier map drawn in the plane C1-N7-C16 showing the the H atom attached to N7 on $[TBP_8CzH_4]^+$.

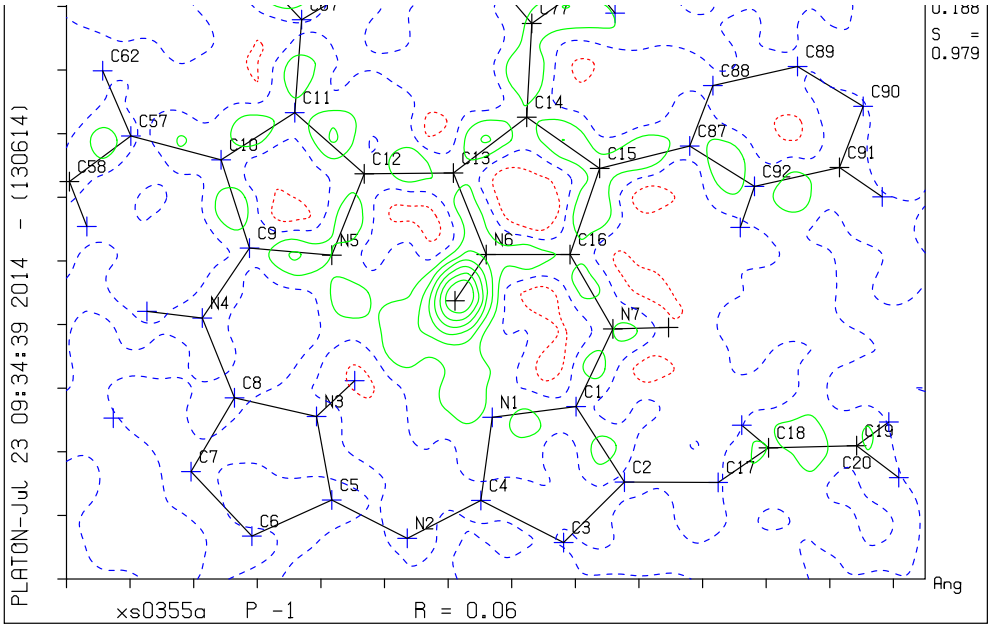

Figure S6. Electron density difference Fourier map drawn in the plane C13-N6-C16 showing the the H atom attached to N6 on $[TBP_8CzH_4]^+$.

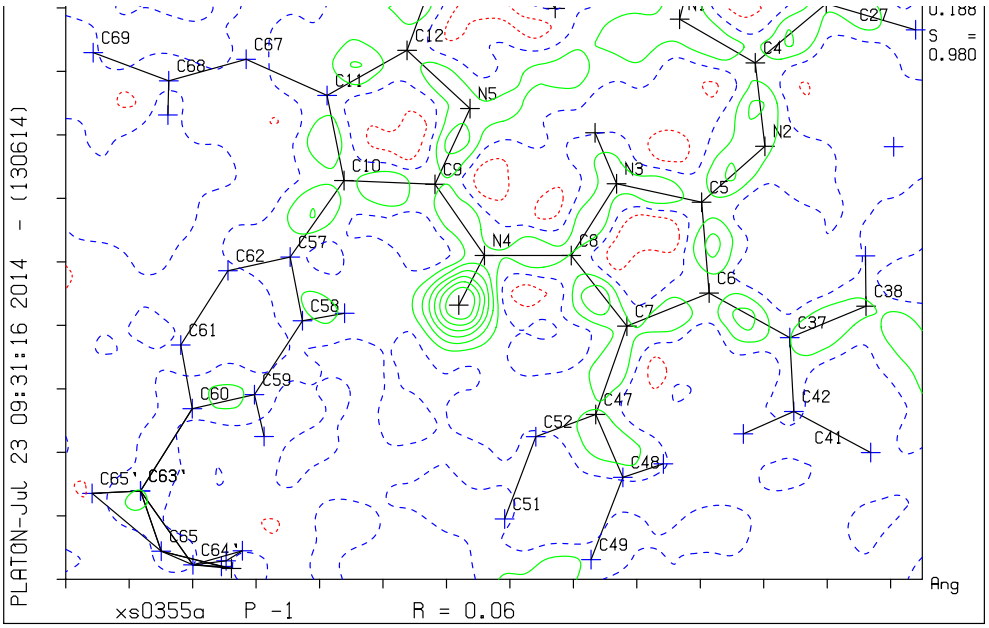

Figure S7. Electron density difference Fourier map drawn in the plane C8-N4-C9 showing the the H atom attached to N4 on $[TBP_8CzH_4]^+$.

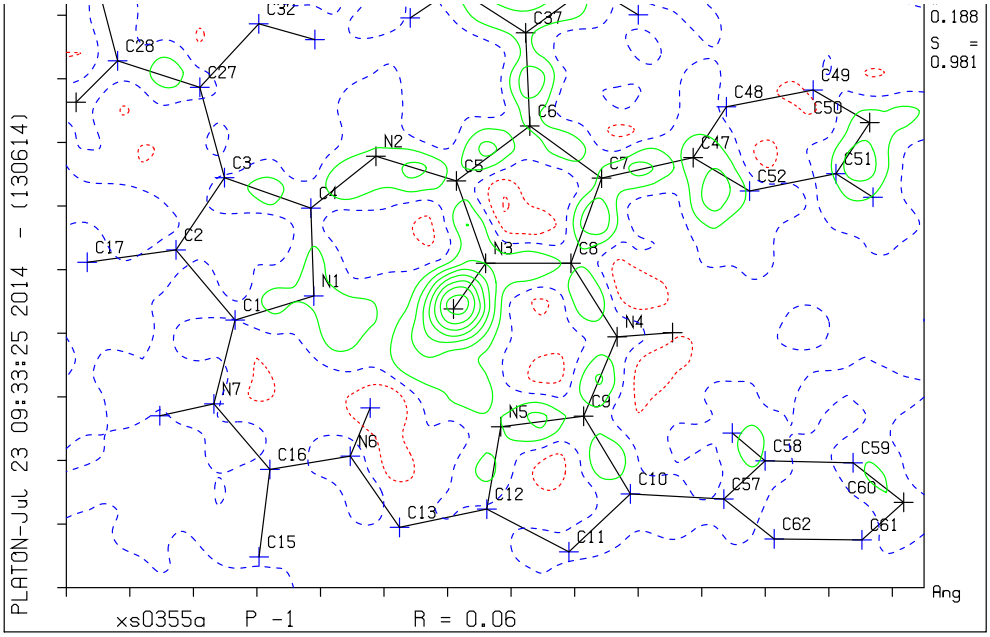

Figure S8. Electron density difference Fourier map drawn in the plane C5-N3-C8 showing the the H atom attached to N3 on $[TBP_8CzH_4]^+$.

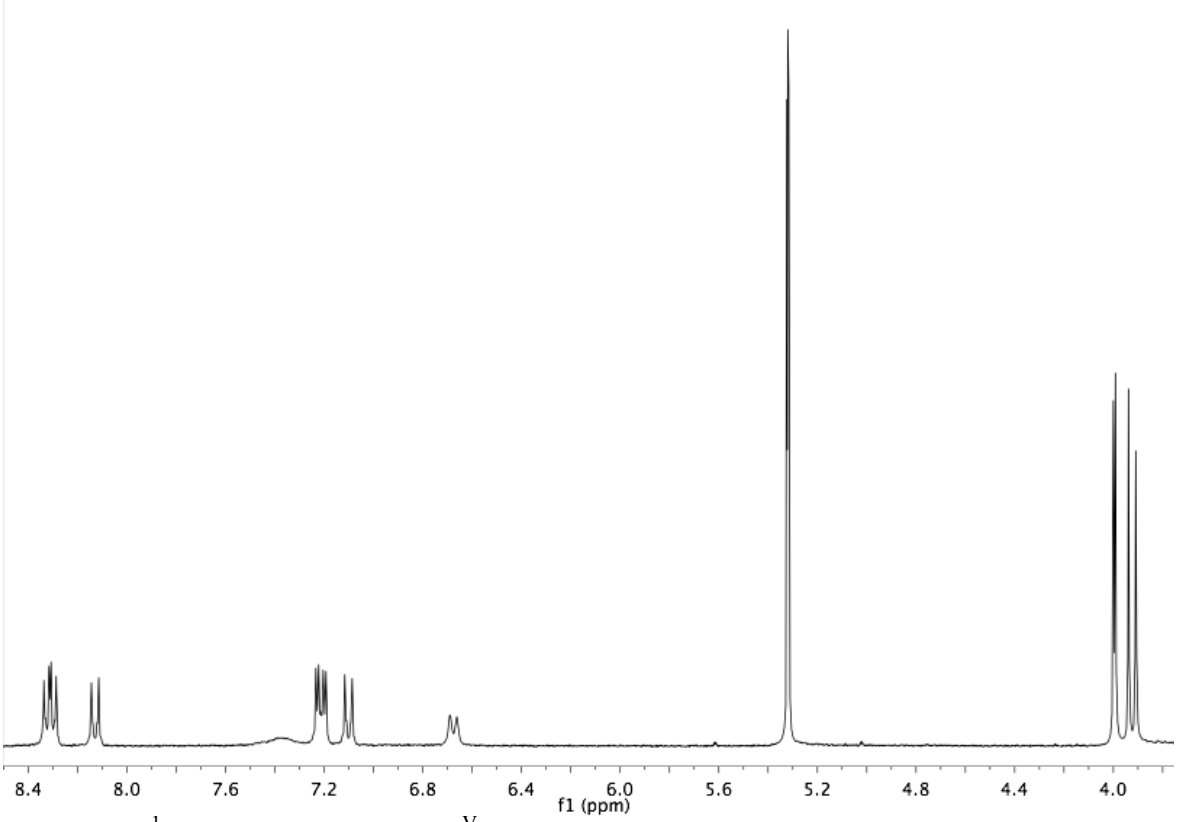

Figure S9. ^{1}H NMR spectrum of [P^{V}(MeOP_8Cz)(OH)]OH in CD_2Cl_2.

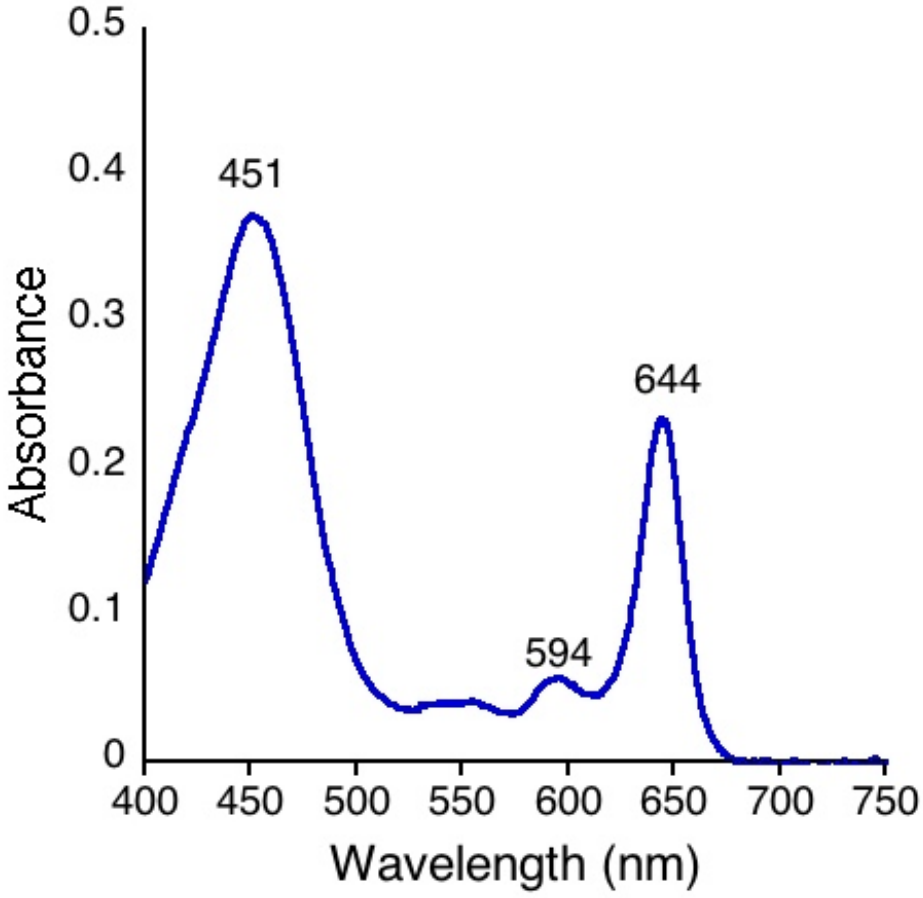

Figure S10. UV-vis spectrum of P^{V}(MeOP_8Cz)$(OMe)_2$ in CH_2Cl_2.

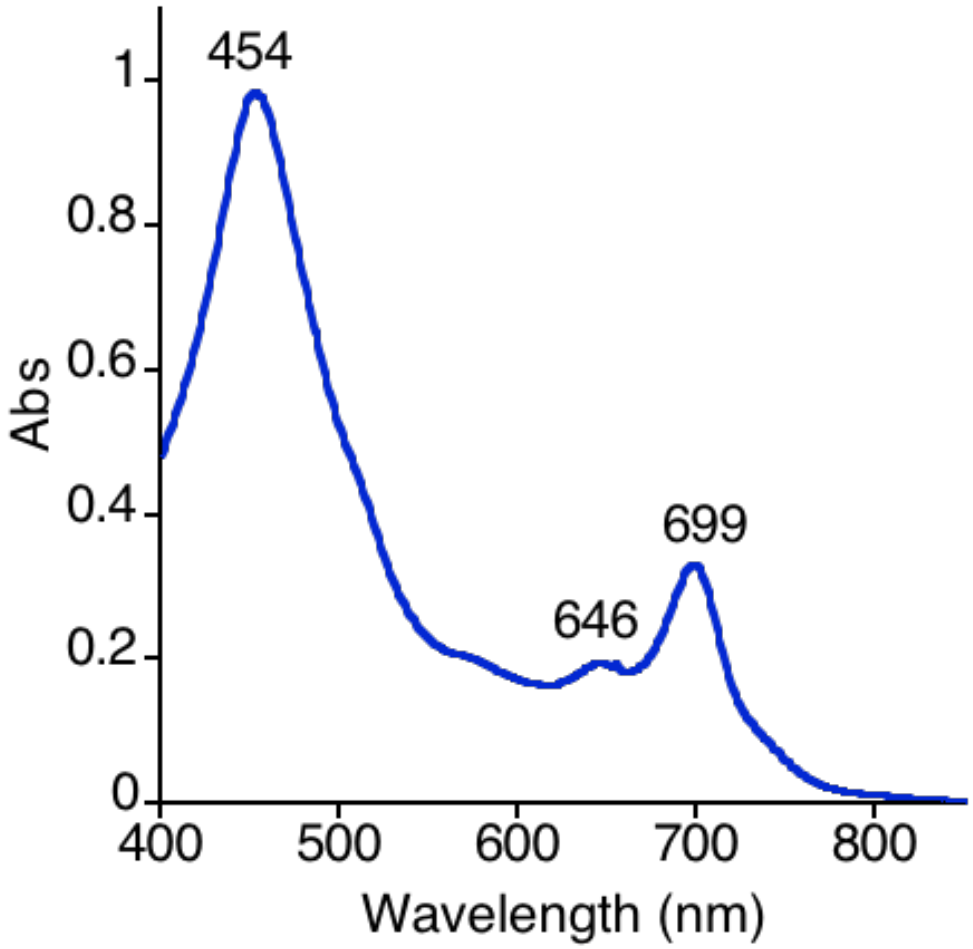

Figure S11. UV-vis spectrum of $Mn^{III}(MeOP_8Cz)(pyr)$ in $CHCl_3$.

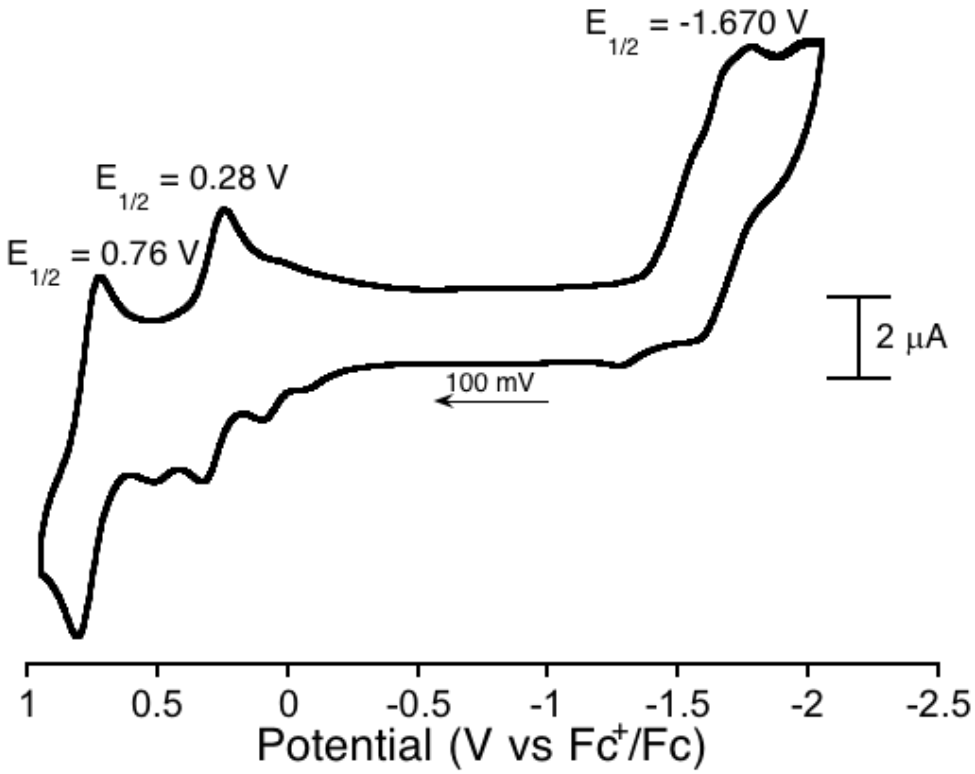

Figure S12. Cyclic voltammogram for $Mn^{III}(TBP_8Cz)$ (0.3 mM) in CH_2Cl_2 with 0.1 M Bu_4N electrolyte.

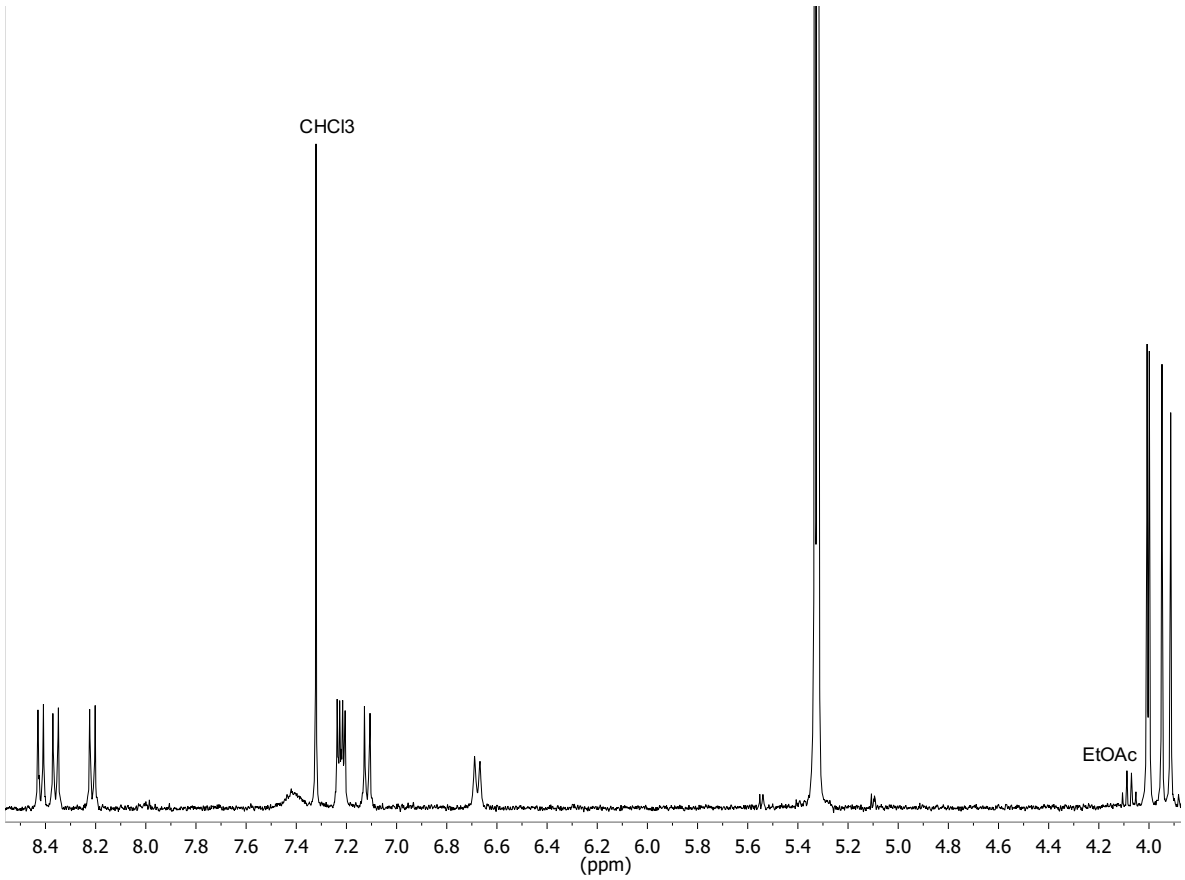

Figure S13. ^{1}H NMR spectrum of $Mn^{V}(O)(MeOP_8Cz)$ in CD_2Cl_2.

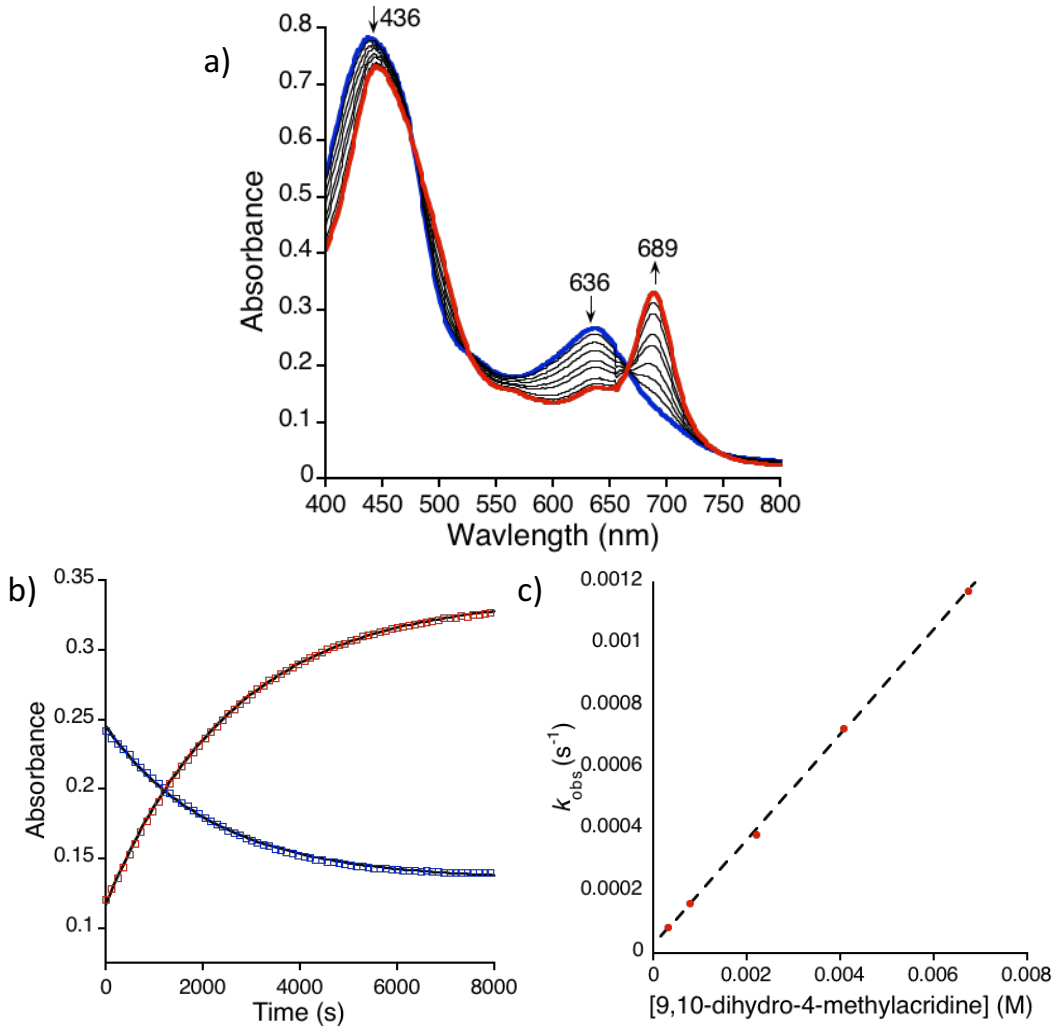

Figure S14. a) Time-resolved UV-vis spectral changes observed in the reaction of $Mn^{V}(O)(MeOP_8Cz)$ (16 μM) with 9-methyl-9,10-dihydroacridine (2 mM) in CH_2Cl_2 at 25 °C. b) Changes in absorbance vs time for the growth of $Mn^{III}(MeOP_8Cz)$ (red circles) and decay of $Mn^{V}(O)(MeOP_8Cz)$ (blue squares) with the best fit lines (black). c) Plots of pseudo-first-order rate constants (k_{obs}) versus [9-methyl-9,10-dihydracridine] ($R^2 = 0.99$).

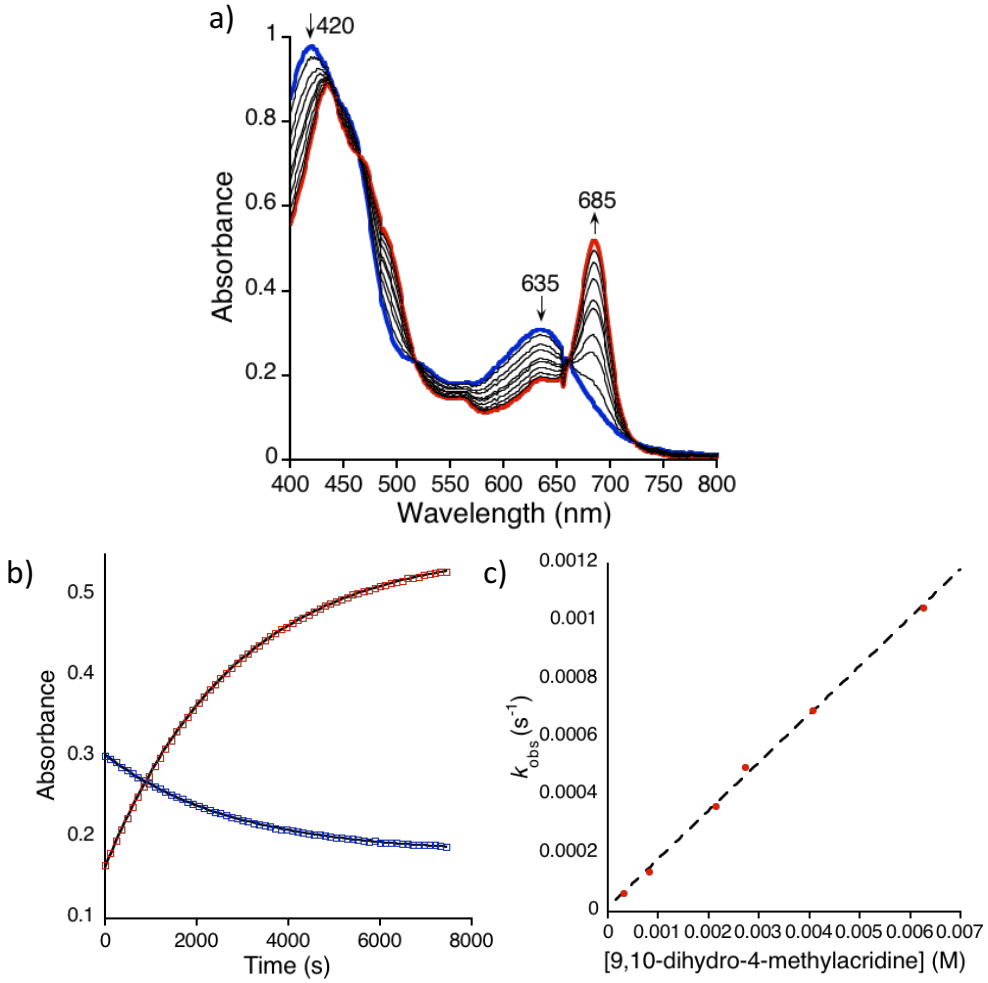

Figure S15. a) Time-resolved UV-vis spectral changes observed in the reaction of $Mn^{V}(O)(TBP_8Cz)$ (15 μM) with 9-methyl-9,10-dihydracridine (2 mM) in CH_2Cl_2 at 25 °C. b) Changes in absorbance vs time for the growth of $Mn^{III}(TBP_8Cz)$ (red circles) and decay of $Mn^{V}(O)(TBP_8Cz)$ (blue squares) with the best fit lines (black). c) Plots of pseudo-first-order rate constants (k_{obs}) versus [9-methyl-9,10-dihydracridine] ($R^2 = 0.99$).

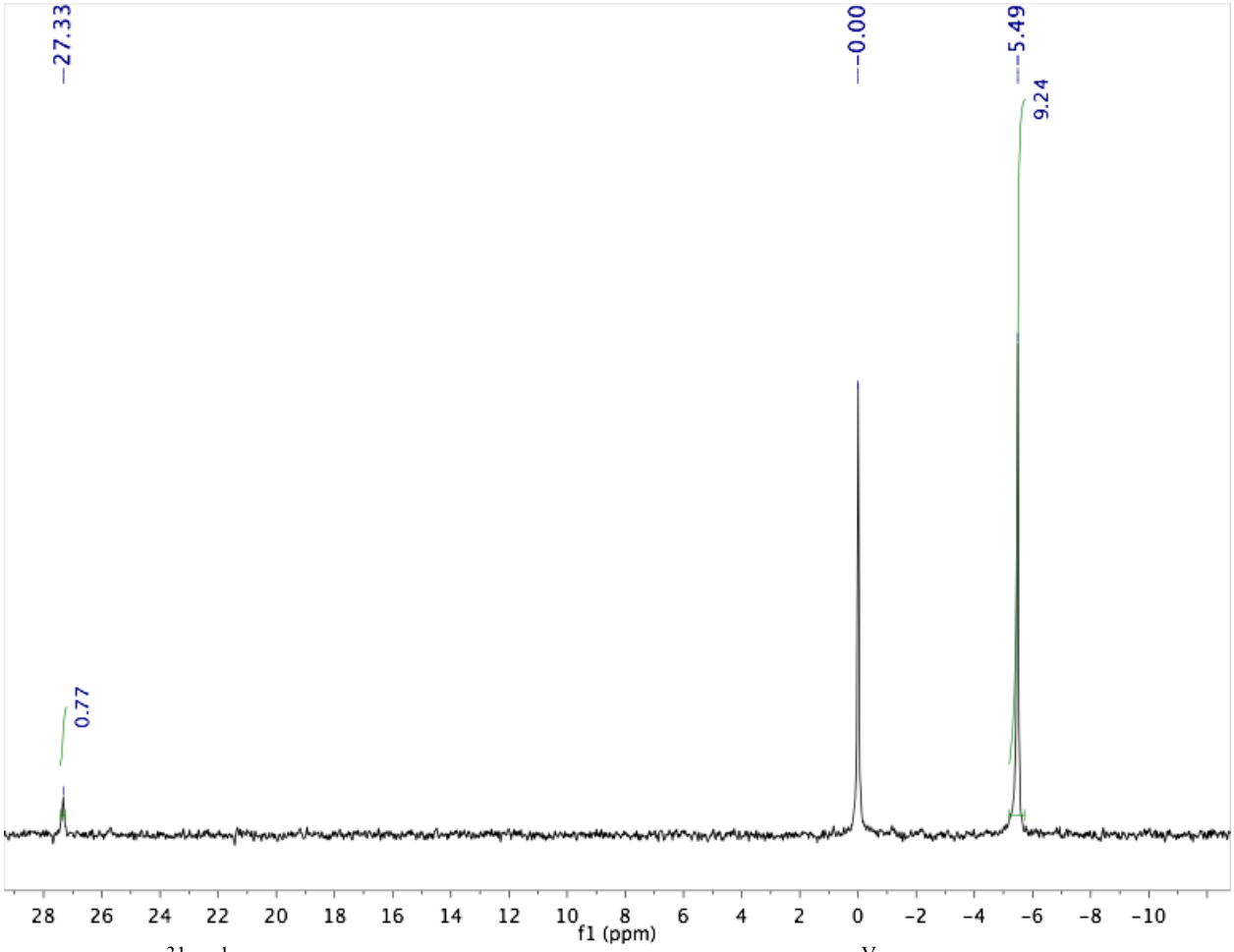

Figure S16. $^{31}P\{^{1}H\}$ NMR spectrum for the reaction mixture of $Mn^{V}(O)(MeOP_8Cz)$ + 10 PPh_3 after addition of excess $Bu_4N^+F^-$ in CD_2Cl_2. Peaks for PPh_3 (δ = -5.5 ppm) and $OPPh_3$ (δ = 27.3 ppm) were observed. A yield of 77% for $OPPh_3$ was obtained by comparison of the integration for PPh_3 and $OPPh_3$. External standard H_3PO_4 seen at 0.00 ppm.